

PAPER • OPEN ACCESS

Correlation between frequency and location on the wafer for terahertz quantum-cascade lasers

To cite this article: Xiang Lü *et al* 2021 *Semicond. Sci. Technol.* **36** 035012

View the [article online](#) for updates and enhancements.

You may also like

- [Excitation of relaxation oscillations due to a shift of the emission frequency of a CO₂ laser](#)

N A Gryaznov, V M Kiselev and E N Sosnov

- [Tunable electron-beam-controlled carbon dioxide laser](#)

N G Basov, E M Belenov, V A Danilychev et al.

- [Submillimeter backward-wave tube frequency-locked to an HCOOH laser for use in a submillimeter spectrometer](#)

V F Zakhar'yash, V M Klement'ev, P A Losev et al.

Correlation between frequency and location on the wafer for terahertz quantum-cascade lasers

Xiang Lü , Benjamin Röben , Lutz Schrottke , Klaus Biermann  and Holger T Grahn 

Paul-Drude-Institut für Festkörperelektronik, Leibniz-Institut im Forschungsverbund Berlin e.V., Hausvogteiplatz 5–7, 10117 Berlin, Germany

E-mail: lue@pdi-berlin.de

Received 18 November 2020, revised 12 January 2021

Accepted for publication 19 January 2021

Published 5 February 2021



Abstract

We have investigated the emission frequency of terahertz (THz) quantum-cascade lasers (QCLs) as a function of the location on the wafer. The frequency varies due to an inhomogeneous growth rate across the wafer. For three wafers based on GaAs/AlAs heterostructures for lasers with target frequencies of 3.36 and 3.92 THz, we observed a blue shift of the emission frequency from the center to the edge of the wafer. This blue shift is attributed to a decrease of the period length of the QCLs, which can be determined with spectroscopic techniques. The location-dependent period length is used to calculate a position-dependent frequency of the gain maximum for the active region. The correlation of the calculated frequencies with the emission frequencies of lasers fabricated from different locations on the wafer allows us to establish an effective method for the fabrication of THz QCLs emitting at a particular target frequency.

Keywords: terahertz quantum-cascade lasers, emission frequency, growth rate, GaAs/AlAs

1. Introduction

High-resolution spectroscopy in the terahertz (THz) spectral range is a promising tool for the detection and investigation of atoms, ions, and molecules, since many fine-structure transitions and transitions between rotational states lead to absorption or emission of THz radiation. While absorption lines can be determined by measuring the transmission of the radiation through an absorption cell as a function of the frequency of a tunable source, emitted radiation can be detected by heterodyne spectrometers, in which a difference frequency is generated by superimposing the received signal

with radiation from a local oscillator. For both approaches, radiation sources with well-defined emission frequencies and a sufficient frequency tuning of several gigahertz (GHz) are required. Due to the high emission powers and narrow line widths in continuous-wave (cw) operation, THz quantum-cascade lasers (QCLs) [1–5] are promising sources for both applications. As examples, the transition between rotational states of the hydroxyl radical (OH) at 3.55 THz and the fine-structure transition of neutral atomic oxygen (OI) at 4.75 THz are of current interest in astronomy and planetary science. These spectral lines can be measured by a heterodyne spectrometer using a THz QCL in a local oscillator [6–12]. Furthermore, THz QCLs are expected to be suitable radiation sources for the detection of Si, Al, N⁺, and O atoms/ions in plasma processes by high-resolution absorption spectroscopy of the respective fine-structure transitions at 2.31, 3.36, 3.92, and 4.75 THz [13]. Alternatively, frequency combs based on THz QCLs [14, 15] would allow for broad-band THz spectroscopy. Recently, significant progress in the development



Original Content from this work may be used under the terms of the [Creative Commons Attribution 4.0 licence](#). Any further distribution of this work must maintain attribution to the author(s) and the title of the work, journal citation and DOI.

of high-temperature operation of THz QCLs in pulsed mode has been reported [16, 17], which paves the way for further real-world applications.

THz QCLs are based on rather complex semiconductor heterostructures with more than 1000 layers, reaching a total thickness of more than $10 \mu\text{m}$. These heterostructures are grown by molecular beam epitaxy (MBE). The frequency of the gain maximum is basically determined by the layer sequence of the heterostructure design, which is achieved by appropriate shutter opening times for the given growth rates. Due to the nominally very thin barrier layers down to a single monolayer, GaAs/AlAs QCLs are grown at a rather low growth rate of around 0.13 nm s^{-1} , which leads to extended growth times on the order of 25 h for a complete QCL layer stack. They are typically grown at a substrate temperature of 600°C on semi-insulating GaAs (001) substrates under a V/III beam equivalent pressure of 20. However, the growth conditions may significantly affect the operating parameters. We found that the growth rate decreases from the center to edge of the wafer by up to 3.0%. This inhomogeneity of the thickness of the active region and, hence, of the period length corresponds to a variation of the gain spectrum across the wafer. A well-determined dependence of the emission frequency on the location of the wafer investigated by both, experiments and simulations, allows for a rather efficient development of THz QCLs with application-defined emission frequencies. Instead of growing several wafers with slightly varying period lengths for the active regions, we make use of their variation across one wafer in order to obtain lasers emitting at the target frequency.

2. Methods

THz QCLs based on GaAs/AlAs heterostructures were grown on two-inch wafers in an MBE system (VG 8-port V80H) under continuous wafer rotation so that only the dependence of the growth rate along the radial direction has to be considered, which is determined using spectral reflectivity measurements. The lasers are based on single-plasmon waveguides and processed by photo-lithography and standard wet chemical etching. Their operating parameters were determined under cw or pulsed operation in a helium flow cryostat (Oxford Optistat CF-V). The lasing spectra were recorded using a Fourier-transform infrared spectrometer (Bruker Vertex 80v), while the output power was determined using a calibrated power meter (Laser Probe RkP-575 RF).

We investigated lasers fabricated from three wafers A–C at several positions on these wafers. The target frequency for wafer A is 3.36 THz, while it is 3.92 THz for wafers B and C. The details of the design of wafer A are given in¹, while the

details for wafers B and C are given in^{2,3}, respectively. Lasers with ridge dimensions of approximately $0.12 \times 1.0 \text{ mm}^2$ exhibit one or two dominant emission peaks and are operated in cw mode, while lasers with ridge dimensions of about $0.20 \times 3.0 \text{ mm}^2$ exhibit multi-mode spectra and are investigated in pulsed mode with a pulse length of 500 ns and a repetition rate of 5 kHz, i.e. a duty cycle of 0.25%.

For a better comparison of the operating parameters for lasers in cw mode with the ones for lasers operating in pulsed mode, we adjusted the heat sink temperature T_{hs} , since cw and pulsed mode exhibit different thermal conditions, so that the expected temperatures of the active regions are as similar as possible for both cases. Assuming a monotonous dependence of the threshold current density on the active-region temperature, we applied the following procedure. For a laser with a cavity length of about 1 mm, we recorded first the threshold current density under cw operation for $T_{hs} = 30 \text{ K}$, i.e. $J_{th,cw}(30 \text{ K})$. Then, we measured for the same laser the temperature-dependent light output-current density-voltage characteristics under pulsed operation and obtained the threshold current density as a function of T_{hs} , i.e. $J_{th,pulsed}(T_{hs})$. By comparing the curve of $J_{th,pulsed}(T_{hs})$ with the value of $J_{th,cw}(30 \text{ K})$, we obtained $J_{th,cw}(30 \text{ K}) \approx J_{th,pulsed}(50 \text{ K})$. Therefore, lasers under pulsed operation were measured at $T_{hs} = 50 \text{ K}$, while lasers under cw operation were measured at $T_{hs} = 30 \text{ K}$, so that similar active-region temperatures are ensured.

In order to correlate the frequency shift along the radial direction of the wafer with the position-dependent period length, we calculated the gain spectra and determined the frequency of the gain maxima for different period lengths in the framework of a self-consistent Fourier-transform-based transport model [18–20]. First, we slightly rescaled the period length of the nominal design (d_p^{des}) so that the simulated frequency of the gain maximum (ν_{max}^{sim}) is close to the emission frequency of a laser under cw operation fabricated from a piece near the center of the wafer. We labeled this thickness as $d_{p,cen}^{sim}$ and the corresponding frequency as $\nu_{max,cen}^{sim}$. Then, we simulated gain spectra for different values of $d_p^{sim} (< d_{p,cen}^{sim})$. According to the relation between the period length and the location on the wafer, we obtained the gain spectra as a function of the location on the wafer.

3. Results and discussion

Figure 1 depicts the relative change in the growth rate r_g across wafer A with respect to the growth rate at the center of the

² Wafer B corresponds to sample PDI-M4-3417. The layer sequence starting from the injection barrier is **1.12**, 29.9, **0.56**, 16.1, **0.42**, 12.8, **0.42**, 11.3, **0.42**, 9.6, **0.42**, 8.8, **0.42**, 19.1, **0.84**, 19.1 with the layer thicknesses in nm. Bold numbers denote the AlAs barriers, while the underlined number indicates the doped layer. The nominal doping density is $1.5 \times 10^{17} \text{ cm}^{-3}$.

³ Wafer C corresponds to sample PDI-M4-3440. The layer sequence starting from the injection barrier is **1.12**, 29.9, **0.56**, 16.1, **0.42**, 12.8, **0.42**, 11.3, **0.42**, 9.6, **0.42**, 8.8, **0.42**, 19.1, **0.96**, 19.1 with the layer thicknesses in nm. Bold numbers denote the AlAs barriers, while the underlined number indicates the doped layer. The nominal doping density is $2.0 \times 10^{17} \text{ cm}^{-3}$.

¹ Wafer A corresponds to sample PDI-M4-3478. The layer sequence starting from the injection barrier is **1.12**, 33.1, **0.56**, 16.3, **0.42**, 13.1, **0.42**, 11.7, **0.42**, 10.5, **0.42**, 9.3, **0.42**, 20, **0.84**, 19.6 with the layer thicknesses in nm. Bold numbers denote the AlAs barriers, while the underlined number indicates the doped layer. The nominal doping density is $2.0 \times 10^{17} \text{ cm}^{-3}$.

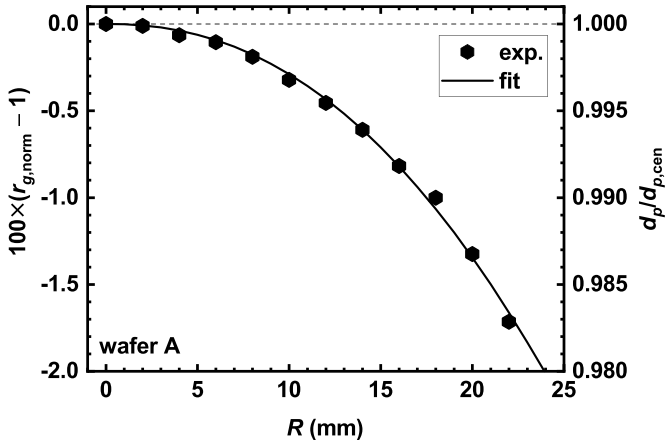


Figure 1. Deviation of the growth rate $r_{g,\text{norm}} - 1$ measured by *ex situ* spectral reflectivity scans as a function of the distance R from the center of wafer A. The corresponding relative period length $d_p/d_{p,\text{cen}}$ is also given on the right-hand side.

wafer $r_{g,\text{cen}}$, i.e. $(r_g - r_{g,\text{cen}})/r_{g,\text{cen}} = r_{g,\text{norm}} - 1$, as a function of the distance R from the center of the wafer, where $r_{g,\text{norm}}$ denotes the normalized growth rate. The right-hand scale in figure 1 shows the location-dependent relative period length $d_p/d_{p,\text{cen}}$ as determined from the normalized growth rate $r_{g,\text{norm}}$. The deviation of $r_{g,\text{norm}}$ was evaluated by *ex situ*, normal-incidence, near-infrared spectral reflectivity scans from the center to the edge of the wafer in steps of 2 mm. Thereby, the spectral positions of minima and maxima in the near-infrared spectral range are extracted [21]. Corresponding to the slightly decreasing growth rate from the center to the edge, the reflectivity minima and maxima shift to lower wavelengths in that scan direction. Taking the wavelength-dependent refractive index into account, the observed relative change in optical thickness can be translated into the relative change of both, the period length and the growth rate, so that we are able to determine the deviation of $r_{g,\text{norm}}$ at any point along the radial direction. The relation between $d_p/d_{p,\text{cen}} - 1$ and R can be well reproduced by a power law given by

$$d_p/d_{p,\text{cen}} - 1 = -C(R/\text{mm})^a \quad (1)$$

with the characteristic parameters $C = 1.74 \times 10^{-5}$ and $a = 2.22$, which is indicated by the solid line in figure 1.

We measured eight QCLs fabricated from wafer A, which are located in different regions of the wafer ($1 \text{ mm} < R < 20 \text{ mm}$). Figure 2(a) displays the distance R from the center of the wafer for the QCLs on wafer A as a function of the emission frequency. The widths of the rectangles in figure 2(a) depict the intrinsic tuning ranges of the laser modes due to changes in the driving current. For laser A7 under pulsed operation (magenta rectangle), which exhibits a two-mode spectrum, the mode with the maximum intensity was selected as shown in figure 2(b). Note that the emission spectra of this laser at $T_{\text{hs}} = 10$ and 30 K exhibit three emission peaks (not shown). In general, QCLs with a cavity length of about 3 mm exhibit several emission peaks with a smaller mode spacing than for a cavity length of 1 mm so that

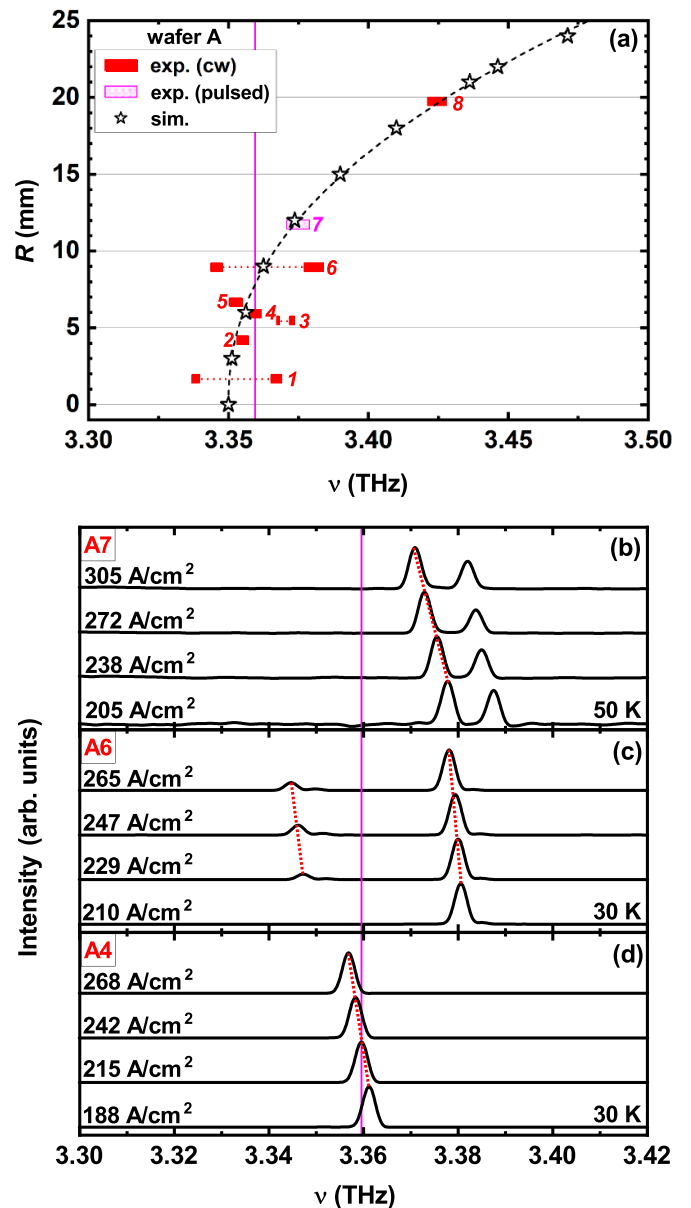


Figure 2. (a) The location of the QCLs on wafer A as a function of frequency measured at $T_{\text{hs}} = 30 \text{ K}$ for cw operation (red rectangles) and $T_{\text{hs}} = 50 \text{ K}$ for pulsed operation (magenta rectangle). The horizontal dotted lines connect the dominant peaks for lasers A1, A3, and A6 under cw operation. The simulated results are indicated by asterisks, and the result of the fit is marked by the dashed line. The vertical line marks the target frequency of 3.36 THz. Emission spectra for (b) laser A7 (pulsed operation), as well as (c) and (d) for lasers A6 and A4 (cw operation), respectively. The dotted lines indicate the intrinsic tuning ranges due to the changes in driving current.

the gain maxima are close to the lasing modes with maximum intensity. Figures 2(c) and (d) display two examples (lasers A6 and A4) for the determination of the tuning ranges under cw operation. These QCLs with a cavity length of about 1 mm and a larger mode spacing than for a cavity length of 3 mm exhibit one or two emission peaks so that the gain maxima may be located at a certain distance from the emission peak or between two emission peaks. In figure 2(a), the frequencies of

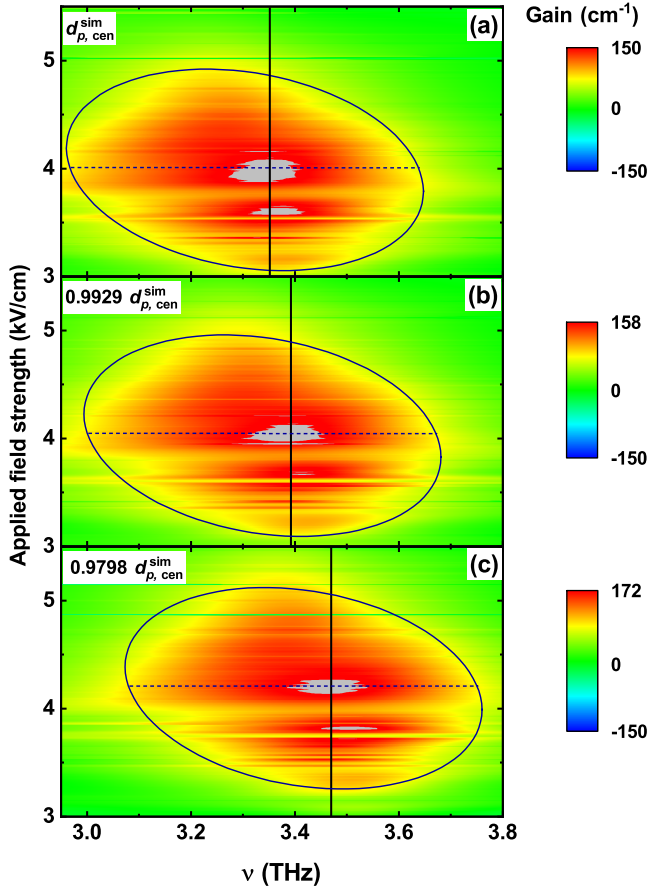


Figure 3. Calculated gain spectra as a function of the applied electric field strength for the period length equal to (a) $d_{p,\text{cen}}^{\text{sim}}$ ($R = 0$), (b) $0.9929 d_{p,\text{cen}}^{\text{sim}}$ ($R = 15 \text{ mm}$), and (c) $0.9798 d_{p,\text{cen}}^{\text{sim}}$ ($R = 24 \text{ mm}$). The marked ellipses depict the ranges with gain values larger than G_{cr} ($G_{\text{cr}} = 65 \text{ cm}^{-1}$ in (a), 73 cm^{-1} in (b), and 84 cm^{-1} in (c)). The vertical lines indicate the position of the gain maximum ν_{\max}^{sim} , while the horizontal dashed lines mark the corresponding applied field strengths.

QCLs with two dominant peaks are connected by horizontal dotted lines to indicate the frequency range of the position of the gain maxima (lasers A1, A3, and A6). The dependence of R on ν shown in figure 2(a) demonstrates that the variation of the growth rate from the center to the edge of the wafer leads to a monotonous blue shift of the emission frequency. The frequency range of laser A4 (3.357–3.362 THz) includes the target frequency of 3.36 THz as also shown in figure 2(d).

Figures 3(a)–(c) display the calculated gain spectra as a function of the applied electric field strength (gain map) for the period lengths of $d_{p,\text{cen}}^{\text{sim}}$, $0.9929 d_{p,\text{cen}}^{\text{sim}}$, and $0.9798 d_{p,\text{cen}}^{\text{sim}}$, respectively, where the rescaled period length $d_{p,\text{cen}}^{\text{sim}}$ is equal to 1.017 times the designed period length d_p^{des} . The shape of the gain map is rather similar for these three period lengths, if the gain scale is adjusted accordingly. This shape can be approximately described by an ellipse, which roughly corresponds to the map areas with the critical gain value G_{cr} as indicated in the caption of figure 3. Regions with maximum gain are

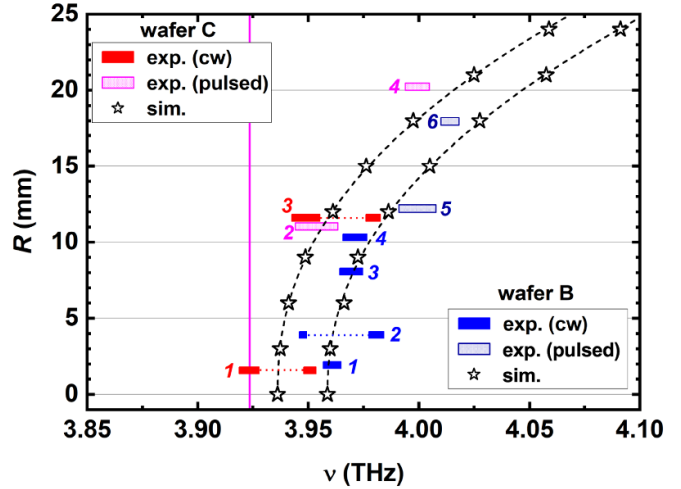


Figure 4. The location of the QCLs as a function of frequency measured at $T_{\text{hs}} = 30 \text{ K}$ under cw operation for wafers B (blue rectangles) and C (red rectangles) and at $T_{\text{hs}} = 50 \text{ K}$ under pulsed operation for wafers B (royal blue rectangles) and C (magenta rectangles). The horizontal dotted lines depict the dominant peaks for lasers B2, C1, and C3 under cw operation. The simulated results are indicated by asterisks, and the results of the fit are given by the dashed lines. The vertical line marks the target frequency of 3.92 THz .

indicated by the gray areas, which appear at a similar position inside the ellipses for all three cases as marked by the dashed lines. The frequencies of the simulated gain maxima (ν_{\max}^{sim}) indicated by the vertical lines in figure 3 correspond to three examples of the asterisks shown in figure 2(a). The horizontal dashed lines in figure 3 indicate the field strength at the simulated gain maximum, which always appear at a similar position with respect to the ellipse, demonstrating the applicability of our method. The decrease of the period length d_p^{sim} results in an increase of the simulated frequency as well as in an increase of the corresponding applied field strength. From the values of ν_{\max}^{sim} as a function of $d_p^{\text{sim}}/d_{p,\text{cen}}^{\text{sim}}$ and the relation between $d_p/d_{p,\text{cen}}$ and the distance R measured by spectral reflectivity scans (cf figure 1), we obtained the simulated frequency as a function of R . We also found that the relation between R and ν_{\max}^{sim} can be well fitted by

$$R(\nu_{\max}^{\text{sim}}) = D \left(\frac{\nu_{\max}^{\text{sim}}}{\nu_{\max,\text{cen}}^{\text{sim}}} - 1 \right)^b \quad (2)$$

with $D = 106.4 \text{ mm}$ and $b = 0.44$. This location function $R(\nu_{\max}^{\text{sim}})$ describes the correlation between the emission frequency of the QCLs and the location on the wafer as indicated by the dashed line in figure 2(a). The simulated frequencies agree well with the experimental results.

In order to demonstrate the broad applicability of our method, we also analysed two QCLs designed for 3.92 THz (wafers B and C). The design of wafer C is similar to that of wafer B, but with a thicker AlAs barrier (0.96 nm instead of 0.84 nm) after the doped layer and a larger Si doping density ($2.0 \times 10^{17} \text{ cm}^{-3}$ instead of $1.5 \times 10^{17} \text{ cm}^{-3}$). Figure 4 displays the location of six (four) QCLs on wafers B (C) as a function of frequency. For wafers B (blue and

royal blue rectangles in figure 4) and C (red and magenta rectangles in figure 4), the change of the frequency with increasing distance R from the center of the wafer has a similar dependence as that for wafer A. Note that the emission spectra of lasers B5, B6, C2, and C4 (pulsed operation) exhibit more than two emission peaks (not shown). The frequency range of one lasing mode of laser C1 (3.919–3.924 THz) includes the target frequency of 3.92 THz. For wafers B and C, we obtain $d_{p,\text{cen}}^{\text{sim}} = 1.028 d_p^{\text{des}}$ and $d_{p,\text{cen}}^{\text{sim}} = 1.032 d_p^{\text{des}}$, respectively. Again, the simulated frequencies along the radial direction labeled by asterisks are in agreement with the experimental frequencies. The relation between R and $\nu_{\text{max}}^{\text{sim}}$ can also be well fitted by equation (2) for wafers B and C. The corresponding parameters are $D = 111.2$ and 109.5 mm as well as $b = 0.45$ and 0.44 , respectively, which are very similar values as for wafer A. By considering the relation between $d_p/d_{p,\text{cen}}$ and $\nu_{\text{max}}^{\text{sim}}/\nu_{\text{max,cen}}^{\text{sim}}$, equation (2) can be correlated with equation (1), and the exponent $b \approx 1/a$.

Using this method, we are now able to predict the covered frequency range for a new wafer and efficiently determine the suitable position on the wafer from which a THz QCL with an application-defined emission frequency is fabricated. Using the design for a particular frequency, one or two lasers from the center of a new wafer are fabricated. Then, we measure the frequencies and determine the values of $d_{p,\text{cen}}^{\text{sim}}$ and $\nu_{\text{max,cen}}^{\text{sim}}$ using the procedure described above. By employing equation (1), we obtain the simulated frequencies $\nu_{\text{max}}^{\text{sim}}$ across the wafer as well as the location function $R(\nu_{\text{max}}^{\text{sim}})$. If the simulated frequency range includes the target frequency ν_{target} , we directly get $R_{\text{target}} = R(\nu_{\text{target}})$. At the distance R_{target} from the center of the wafer, a QCL with a suitable length [22] is expected to emit at the target frequency.

For applications of THz QCLs, the optical output power and the electrical pump power (the product of the driving current and the voltage) are also important operating parameters. For typical applications, optical output powers of several milliwatts are required for instance to pump the mixer in heterodyne receivers, while smaller electrical pump powers allow for operation in mechanical cryocoolers. To show that most of the lasers fabricated at different locations on the wafer exhibit similar operating parameters, figure 5 summarizes the maximum output power and the electrical pump power of 13 GaAs/AlAs QCLs from wafers A, B, and C as a function of the emission frequency. The threshold current densities vary between 125 and 200 A cm^{-2} . The typical output powers of these lasers (except A3) are larger than 1 mW. For the 3.92-THz QCLs, the maximum electrical pump power is about 3.9 W, while for the 3.36-THz QCLs it is about 1.4 W. The cooling capacity of the Stirling cryocooler (Ricor K535) at 48 K is about 4 W indicated by the dashed line in figure 5(b) [23]. Therefore, all these lasers can be operated in a cryocooler. Some of the 3.36-THz QCLs may even be operated in a miniature cryocooler (AIM SL400) [12], which has a cooling capacity of 1.2 W at 40 K indicated by the dash-dotted line in figure 5(b). The lasers A4 and C1, which exhibit the highest output powers at 3.36 and 3.92 THz, respectively, reach wall plug efficiencies of about 1.6×10^{-3} as well as 0.6×10^{-3} and have intrinsic tuning ranges of 5.0 as well

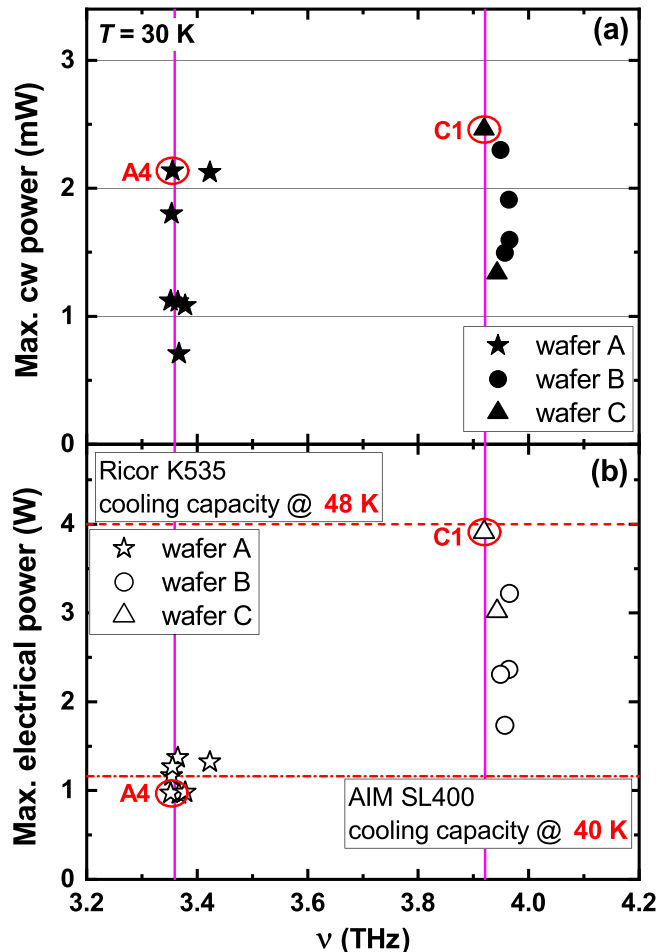


Figure 5. (a) Maximum output power and (b) maximum electrical pump power as a function of the emission frequency for 13 GaAs/AlAs QCLs (symbols) from wafers A, B, and C under cw operation measured at a heat sink temperature of 30 K. The vertical lines indicate the target frequencies of 3.36 and 3.92 THz. The circles indicate the lasers A4 and C1, which emit at the target frequencies of 3.36 and 3.92 THz, respectively. The horizontal dashed (dashed-dotted) line indicate the cooling capacity of a cryocooler (miniature cryocooler) of 4 W (1.2 W).

as 5.4 GHz, respectively. Due to a sufficient output power, a small electrical pump power, and an adequate frequency tunability, these lasers can be used for high-resolution absorption spectroscopy.

4. Conclusions

The correlation between the emission frequency and the location on the wafer due to an inhomogeneous growth rate was investigated for GaAs/AlAs THz QCLs using a combination of experimental work and Fourier-transform-based simulations. The decrease of the growth rate from the center to the edge of the wafer leads to a blue shift of the emission frequency. The experimental frequency shift was well reproduced by simulations, which allows for the determination of the suitable location on the wafer for a given frequency. Rather than growing several homogeneous wafers with a wafer-to-wafer variation

of the nominal active-region thickness, THz QCLs with customized emission frequencies can be efficiently fabricated by making use of this frequency shift across the wafer.

Acknowledgments

The authors would like to thank W Anders, C Herrmann, A Riedel, and A Tahraoui for sample preparation as well as T Flissikowski for a careful reading of the manuscript. Partial financial support of this work by the Leibniz-Gemeinschaft under Grant No. K54/2017 is gratefully acknowledged.

ORCID iDs

Xiang Lü  <https://orcid.org/0000-0001-7169-7771>
 Benjamin Röben  <https://orcid.org/0000-0003-4356-5741>
 Lutz Schrottke  <https://orcid.org/0000-0002-0910-9163>
 Klaus Biermann  <https://orcid.org/0000-0003-4804-0784>
 Holger T Grahn  <https://orcid.org/0000-0001-5451-3950>

References

- [1] Faist J, Capasso F, Sivco D L, Sirtori C, Hutchinson A L and Cho A Y 1994 *Science* **264** 553
- [2] Köhler R, Tredicucci A, Beltram F, Beere H E, Linfield E H, Davies A G, Ritchie D A, Iotti R C and Rossi F 2002 *Nature* **417** 156
- [3] Williams B S 2007 *Nat. Photon.* **1** 517
- [4] Scalari G, Walther C, Fischer M, Terazzi R, Beere H, Ritchie D and Faist J 2009 *Laser Photonics Rev.* **3** 45
- [5] Sirtori C, Barbieri S and Colombelli R 2013 *Nat. Photon.* **7** 691
- [6] Gao J R et al 2005 *Appl. Phys. Lett.* **86** 244104
- [7] Hübers H-W, Pavlov S G, Semenov A D, Köhler R, Mahler L, Tredicucci A, Beere H E, Ritchie D A and Linfield E H 2005 *Opt. Express* **13** 5890
- [8] Kloosterman J L et al 2013 *Appl. Phys. Lett.* **102** 011123
- [9] Schrottke L et al 2013 *Semicond. Sci. Technol.* **28** 035011
- [10] Richter H, Wienold M, Schrottke L, Biermann K, Grahn H T and Hübers H-W 2015 *IEEE Trans. Terahertz Sci. Technol.* **5** 539
- [11] Hübers H-W, Richter H and Wienold M 2019 *J. Appl. Phys.* **125** 151401
- [12] Hagelschuer T, Richter H, Wienold M, Lü X, Röben B, Schrottke L, Biermann K, Grahn H T and Hübers H-W 2019 *IEEE Trans. Terahertz Sci. Technol.* **9** 606
- [13] Schrottke L et al 2020 *IEEE Trans. Terahertz Sci. Technol.* **10** 133
- [14] Burghoff D et al 2014 *Nat. Photon.* **8** 462
- [15] Rösch M, Scalari G, Beck M and Faist J 2015 *Nat. Photon.* **9** 42
- [16] Bosco L, Francké M, Scalari G, Beck M, Wacker A and Faist J 2019 *Appl. Phys. Lett.* **115** 010601
- [17] Khalatpour A, Paulsen A K, Deimert C, Wasilewski Z R and Hu Q 2021 *Nat. Photon.* **15** 16
- [18] Lü X, Schrottke L, Luna E and Grahn H T 2014 *Appl. Phys. Lett.* **104** 232106
- [19] Schrottke L, Lü X and Grahn H T 2015 *J. Appl. Phys.* **117** 154309
- [20] Lü X, Schrottke L and Grahn H T 2016 *J. Appl. Phys.* **119** 214302
- [21] Biermann K, Helgers P L J, Crespo-Poveda A, Kuznetsov A S, Röben B, Lü X, Schrottke L, Santos P V and Grahn H T 2021 *J. Cryst. Growth* **557** 125993
- [22] Röben B, Lü X, Biermann K, Schrottke L and Grahn H T 2019 *J. Appl. Phys.* **125** 151613
- [23] Richter H et al 2010 *Opt. Express* **18** 10177